RSC Advances

ROYAL SOCIETY OF CHEMISTRY

www.rsc.org/advances

RSC Advances

RSCPublishing

Review

Doped Graphene: Synthesis, Properties and Bioanalysis

Cite this: *RSC Advances*, 2015, **x**, xxxx

Wenyan Zhang, Longfei Wu, Zhaolong Li and Yang Liu*

Received ooth January 2015,
Accepted ooth January 2015

DOI: 10.1039/xoxx00000x

www.rsc.org/ advances

Graphene has attracted an enormous amount of interest because of its excellent properties. The relatively versatile possibility in the doping of graphene sheets affords them tuneable electronic properties, and provides a simple but efficient approach in tuning their catalytic activity at atomic level. Recently, a lot of efforts have been carried out to further tailor the electronic and catalytic properties of graphene by doping, realizing the precise structure control and superior characteristics on graphene, which also broaden their applications in nanoelectronics and optoelectronics. In this review, the synthesis methods developed during last decade on the fabrication of doped graphene with excellent properties are summarized. Moreover, as a rising and brilliant research direction, the bioanalysis applications based on the doped graphene also were demonstrated.

Department of Chemistry, Beijing Key Laboratory for Microanalytical Methods and Instrumentation, Tsinghua University, Beijing 100084, P. R. China. E-mail: liu-yang@mail.tsinghua.edu.cn. Tel: 86-10-62798187

1. Introduction

Graphene is a two-dimensional monolayer of sp^2-hybridized carbon atoms arranged on a honeycomb lattice. Since its discovery in 2004, [1] graphene has aroused enormous amount of interest because of its unique physical and chemical properties such as superior mechanical strength, good thermal conductivity, [2] high surface area, [3] excellent electron transfer rate and ease of functionalization. [4,5] These properties provide possibilities for many potential applications including Field-Effect Transistors (FETs), supercapacitors and sensors. The properties and morphologies of graphene obtained via different methods are distinct from each other. For example, graphene made from chemical vapor deposition (CVD), a bottom-up approach, are generally single and few-layer sheets and possesses large surface area, high-quality and outstanding electrical conductivity and optical transparency. As a while, graphene made from Exfoliation, a top-down approach, is in terms of high yield and ease of implementation. [2] In addition, the properties of graphene are reflected by its structure. As the *s*, p_x and p_y atomic orbitals on each carbon atom in graphene form three strong σ bonds with other three surrounding atoms, the remaining p_z orbital on each carbon atom is overlapped with that on neighbouring carbon atoms to produce a filled band of π orbitals (the valence band) and an empty band of π^* orbitals (the conduction band). When the valence bands (VB) and conduction bands (CB) touch at the Brillouin zone corners, the Fermi level of graphene locates near the Dirac point, shown in Fig. 1A. Consequently, the pristine graphene is a zero-band-gap semimetal, [6] which limits its potential use in electronic and biosensing applications. Hence, many methods have been proposed to tune the band gap by shifting of the Dirac point relative to the Fermi level. When Dirac point is above (below) the Fermi level, the *p*-type (*n*-type) doping graphene can be obtained (Fig. 1B). [7,8,106] Among these methods, chemical doping is an effective approach.

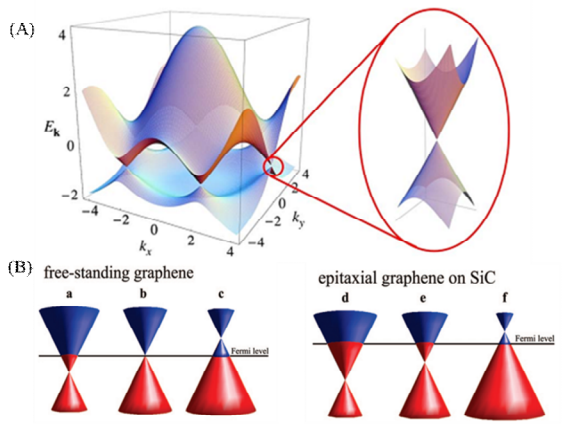

Fig. 1 (A) Left: electronic dispersion in the honeycomb lattice. Right: zoom-in of the energy bands close to one of the Dirac points. (B) A schematic diagram of the position of the Dirac point and the Fermi level as a function of doping. Left: *n*-type doped, pristine and *p*-type doped free standing graphene (a to c). Right: *n*-type doped, pristine and *p*-type doped epitaxial graphene grown on silicon carbide (SiC) (d to f). Reprinted with permission from ref. 6, Copyrights (2011) Royal Society of Chemistry.

Chemical doping can be classified into two categories, surface transfer doping and substitutional doping. [9] Surface transfer doping is achieved by the charge transfer between graphene and dopants adsorbed on the surface of graphene.

While the highest occupied molecular orbital (HOMO) of a dopant is above the Fermi level of graphene, dopants donate electrons to the graphene layer, resulted in the Dirac points below the Fermi level of graphene and obtained n-type doping. While the lowest unoccupied molecular orbital (LUMO) of the dopant is below the Fermi level of graphene, dopants withdraw electrons to the graphene layer, resulted in the Dirac points above the Fermi level of graphene and obtained *p*-type doping. [6] In most cases, this route doesn't destroy the chemical bonds of graphene. As for substitutional doping, heteroatoms, such as nitrogen atom, boron atom, sulfur atom, replace the carbon atoms in the skeleton and break the structure of graphene. Atoms with fewer valence electrons than carbon, like boron, will lead to *p*-type doped graphene, and atoms with more valence electrons than carbon, like nitrogen, will lead to *n*-type doped graphene.

After doping, the graphene exhibits more fascinating photo-/electronic- properties. Doping will influence the charge distribution of carbon atoms in graphene, which makes graphene as a good substrate for FET fabrication. [10] Moreover, the defects induced during doping process are generally the active centres in graphene for the surface chemical reaction. Thus, the doped graphene usually exhibits excellent catalysis behaviours, which shows great promise in bioanalysis. [11-14]

In this review, we summarize recent works in the preparation of doped graphene and demonstrate their unique properties, which may give a valuable guidance for the preparation of novel doped graphene nanomaterials with controlled structure and tuneable properties (Fig. 2). Furthermore, we demonstrate the bioanalysis applications of the doped graphene for determination of small molecules, proteins and cells. Finally, we discuss the future prospects of doped graphene.

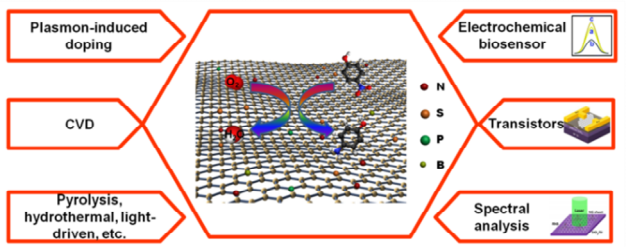

Fig. 2 Synthesis methods of doped graphene and their applications.

2. Synthesis of doped graphene

2.1 Surface transfer doping

For surface transfer doping, molecules with electron withdrawing groups adsorbed on the surface of graphene lead to *p*-type doped graphene, while molecules with electron donating groups adsorbed on the surface of graphene induce *n*-type doped graphene. As graphene has high surface area, it is easy to be absorbed by molecules, including gas, organic molecules and metal atoms.

Water vapor in environment can induce *p*-type doping. Yavari *et al.* [15] reported that the band gap of graphene can be opened when it was exposed to an absolute humidity level. Meanwhile, the amount of water adsorbed on the graphene surface can be controlled precisely by adjusting the absolute humidity level. As this effect was reversible, the bandgap reduced to about 0.029 eV in vacuum. Schedin *et al.* [16] reported that NO_2 molecule is also a strong electron acceptor, which can accept electron from graphene to obtain *p*-type doping. Beside, Br_2 and I_2 are also more electronegative than graphene, inducing *p*-type doping of graphene. [17] As *p*-type graphene can be easily prepared under air and oxygen atmospheres, it is imperative for the complementary circuit to develop *n*-type semiconducting graphene. [18] The molecules with strong donating groups, such as ethanol, NH_3 and CO, can dope graphene with *n*-type. [16]

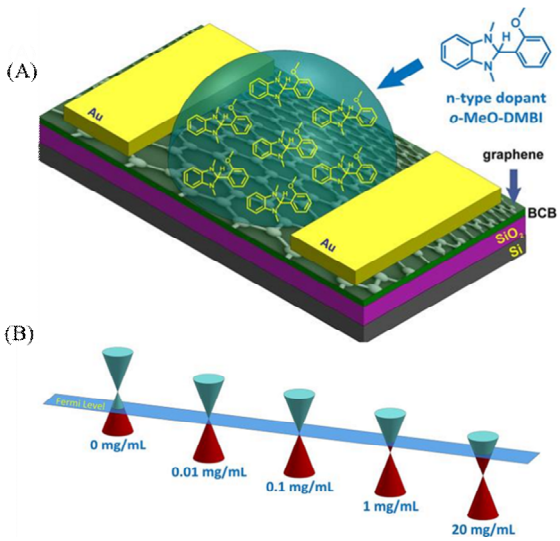

Fig. 3 (A) Chemical structure of *o*-MeO-DMBI and the schematic illustration of *o*-MeO-DMBI doped CVD-grown graphene transistor by solution process. (B) Schematic illustration of the shifts in the Fermi level toward Dirac point varied with the o-MeO-DMBI solution concentrations. Reprinted with permission from ref. 23, Copyrights (2011) American Chemical Society.

Other than gas molecules, organic molecules also have ability to tune the band gap of graphene. Tetrafluoro-tetracyanoquinodimethane (F4-TCNQ) is a strong electron acceptor, which can induce *p*-type doping by adsorbing F4-TCNQ on graphene surface. [19] From synchrotron-based high-resolution photoemission spectroscopy (PES), it was revealed clearly that electron transfer from graphene to F4-TCNQ. Meanwhile, the electron accumulation and depletion only formed at the F4-TCNQ/graphene interface. Tetracyanoethylene (TCNE) [20], tetrasodium 1,3,6,8-pyrenetetrasulfonic acid (TPA) [21] can also adsorb on graphene with *p*-type doping. Avouris' group [22] immersed graphene for 3 h in ethanol solution containing a quantity of PEI at 300 K. As PEI is an amine-rich and electron-donating polymer, graphene doped in *n*-type. Moreover, Wei *et al.* [23] doped graphene utilized the solution of 2-(2-methoxyphenyl)-1,3-dimethyl-2,3-dihydro-1H-benzoimidazole (*o*-MeO-DMBI). By varying the

amount of *o*-MeO-DMBI, it's found that graphene can be controllably tuned from *p*-type to ambipolar and finally *n*-type transport behaviours, shown in Fig. 3. The concentrations of *o*-MeO-DMBI solution make an influence on the relative position between Fermi level and Dirac point.

In addition, metal atoms can also adsorb on graphene to open its band gap. Giovannetti *et al.* [24] used DFT calculations to study the chemical doping graphene induced by adsorption metal on its surface. Due to the difference of work function between graphene and metal atoms, the electrons transfer to equilibrate the Fermi levels when metal atoms adsorb on graphene. For metal-graphene equilibrium separations, graphene is doped with *n*-type on Al, Ag, and Cu, while *p*-type on Au and Pt, shown in Fig. 4A. Other than work function, a graphene-metal chemical interaction also makes a contribution to the charge redistribution at the graphene-metal interface. The chemical interaction depends on the distance between graphene and metal atoms, which was mapped in Fig. 4B.

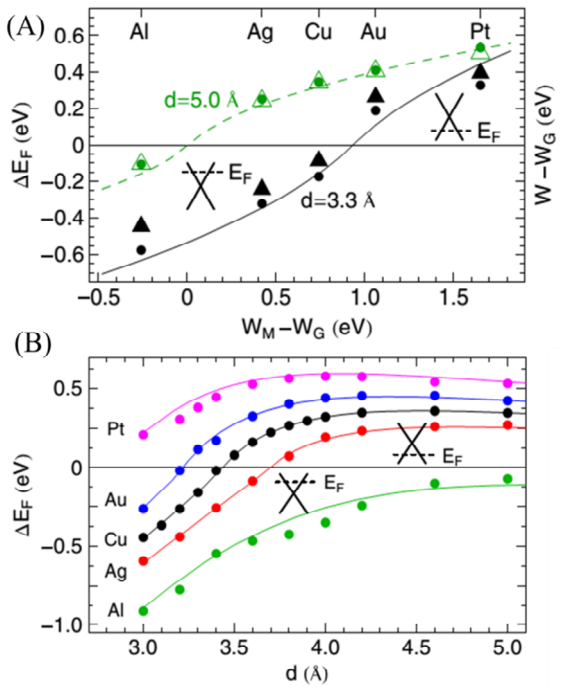

Fig. 4 (A) Calculated Fermi energy shift with respect to the conical point, ΔE_F (dots), and change in the work function $W-W_G$ (triangles) as a function of $W_M - W_G$, the difference between the clean metal and graphene work functions. (B) Fermi level shifts $\Delta E_F(d)$ as a function of the graphene-metal surface distance. The dots give the calculated DFT results, the solid lines give the results obtained from the model. Reprinted with permission from ref. 24, Copyrights (2008) American Physical Society.

2.2 Substitutional doping

Various atoms such as nitrogen, sulfur, phosphorus, boron or transition metals have been introduced into graphene, which change the electron density and broaden their applications in nanodevices and biosensors. Depending on the synthetic process, doped graphene can be prepared by two different methods: direct synthesis and post treatment. The direct synthesis approaches such as chemical vapor deposition (CVD), solvothermal and arc discharge are believed to produce homogeneous doping effects, while post treatments like thermal annealing or plasma treatment may result in surface doping only [25]. The methods developed recently for doped graphene fabrication are summarized in Table 1.

2.2.1 Chemical vapor deposition (CVD)

CVD is one of the most promising methods to prepare doped graphene due to its distinct advantages such as high-quality, large scale, easy transfer and low cost. [26] In this method, metals (i.e. Cu or Ni) are typically needed to grow doped graphene, which act as both the substrate and the catalysts. The precursors are the mixtures of carbon source gas and doping elements containing gas, which then dissociated and recombines into graphene by means of precipitation on the surface of the substrate at high temperatures. In this way, several of doped graphene have been prepared. Despite of the advantages of the CVD method, the high temperature during the doping process may also result in increased defect density or low device performance. Recently, a rapid-heating plasma chemical vapor deposition (RH-PCVD) has been reported by Kato *et al.* [27], which grow carrier-density-controlled graphene on SiO_2 substrate at 600 ºC, much lower than thermal CVD graphene growth (900-1000 ºC). This transport-type tuning of the doping graphene was applied to fabricate FET, in which the charge neutral point can be shifted from the positive to the negative gate bias regions. In addition, Xue *et al.* [28] developed a novel method to grow highly N-doped tetragonal-shaped single crystal graphene (NTSG) arrays by self-assembly of pyridine molecules on Cu surface at 300 ºC under ambient pressure. N-doped graphene in this method was tetragonal-shaped, almost single-layer and single crystal with N content of 16.7%, realized a typical n-type electron doping performance in air.

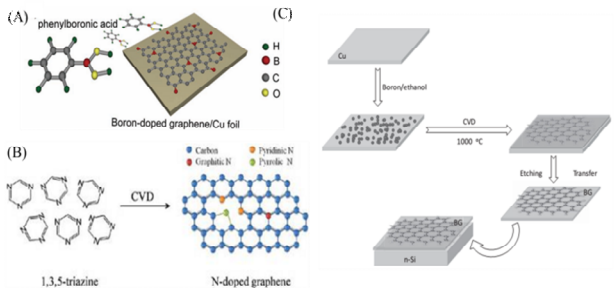

Fig. 5 (A) Schematic diagram of CVD growth of boron-doped graphene. (B) Structures of 1, 3, 5-triazine molecule and N-doped graphene. (C) Schematic of BG preparation. Reprinted with permission from ref. 35, Copyrights (2013) American Chemical Society and from ref. 41, Copyrights (2012) Wiley, respectively.

The doping efficiency of graphene is related to the parameters including catalyst, precursor, flow rate, temperature, pressure and reaction time. [29-34] Controlling the ratio between carbons and doping elements sources can regulate the doping efficiency. However, two precursors may give rise to the uncontrollability of doped graphene growth because of the difference between the source of carbon and doping elements.

As a result, a sole precursor, containing both carbon and doping elements for doped graphene fabrication, was developed recently that can simultaneously introduce chemical species in a controlled manner for the large-scale growth of uniform and high-quality doped graphene. [28, 35, 36] Wang *et al.* [34] synthesized boron-doped graphene on Cu surface by CVD with phenyboronic acid as the carbon and boron sources. Under hydrogen atmosphere, the phenyboronic acid was decomposed into carbonaceous, boron and oxygen species represented by grey, red and yellow, respectively, which was showed in Fig. 5A. The oxygen species were removed by the formation of H_2O or CO_X. Then B-doped graphene film was gradually grown on the copper surface via the graphitization of adsorbed carbonaceous and boron species. In addition, the thickness and the numbers of doped graphene layer can be controlled by adjusting the flowing time of the precursor. [37]

Carbon source play a critical role in the qualities of the doped graphene. Conventional carbon source is CH_4 or C_xH_y. Recently, some organics and polymers, such as pyridine, [38] 1,3,5-triazine [35] or polypyrrole, [39] are also used. Lu *et al.* [35] transferred the conversion of organic molecule triazine into N-doped graphene via CVD method with Cu catalyst. As it was demonstrated in Fig. 5B, doping of graphitic N atoms preserved the high-quality properties of graphene without destroying graphene crystal structure significantly. [40] However, the incorporations of pyridinic and pyrrolic N increased the amount of disorder in the system with structural defects including bonding disorder and vacancies (short-range scatterers). Li *et al.* [41] had successfully incorporated B atoms into graphene sheets by the use of boron powder as the precursor. They regarded the copper foil as substrates to produce the BG films with high transparency on the macroscale. The scheme was exhibited in Fig. 5C. The as prepared B-doped graphene showed *p*-type semiconductor features.

Moreover, Chen's group [105] fabricated nitrogen and sulfur co-doped nanoporous graphene by based CVD. They utilized the nanoporous Ni as both template and substrate, while pyridine and thiophene as carbon, nitrogen and sulfur sources, respectively. As sulfur and nitrogen atom exhibited different electron density distribution, the Fermi level of the doped graphene is negatively shifted to 0.6 eV above the Dirac point, which could obtain high electrical conductivity. Meanwhile, the coupling of S and N dopants introduced geometric defects to the graphene lattice, the Gibbs free energy of H* absorption was tuned and showed the outstanding hydrogen evolution reaction (HER) catalytic ability.

2.2.2 Solvothermal approach

Solvothermal synthesis has been widely used for nanomaterials preparation because of its distinct advantages such as simple operation, mild synthesis conditions, and capability to deliver relatively large quantities. [42] Generally, the dopant-containing precursors act as both the reducing and doping agent in the solvothermal processes. [42,107] For instance, Han *et al.* [43] presented a novel B-doped chemically modified graphene by reduction of graphene oxide with a borane (BH_3)-tetrahydrofuran (THF) adduct under reflux via a one pot process. In addition, N-doped graphene has been reported via one one-step reaction of tetrachloromethane (CCl_4) with lithium nitride (Li_3N). [44] By mixing CCl_4 with Li_3N at 250 ºC for 10h or cyanuric chloride ($N_3C_3Cl_3$) with Li_3N and CCl_4 at 350 °C for 6 h, doped graphene with nitrogen content in the range of 4.5-16.4 at% was obtained. On the other hand, a one-pot solvothermal process were also reported by using graphene oxide (GO) and ammonia boron trifluoride (NH_3BF_3) as precursors via hydrothermal reaction, and a three-dimensional (3D) nitrogen and boron co-doped monolithic graphene aerogels was obtained. [45] The as-prepared 3D doped aerogels show interconnected frameworks with a macroporous architecture, which greatly facilitate ion diffusion and electron transport in bulk electrode.

2.2.3 Arc discharge method

Arc discharge has the advantages of large scale, high quality and purity over the CVD method, which has been widely used to prepare graphene sheets and carbon nanotubes by evaporating the carbon source and graphite at high temperature. [42, 46-48] Rao *et al.* [48] prepared B and N doped graphene by performing the arc discharge of graphite electrodes in the presence of hydrogen (H_2), helium (He), diborane (B_2H_6) or H_2, He, pyridine vapor. However, the dopant content was at very low levels (0.5-1.5 at%). Afterwards, Liu *et al.* [49] introduced a catalytic arc-discharge method by using flake graphite as the carbon source and ZnO or ZnS as catalysts to synthesize N-doped graphene, which the nitrogen content was as high as 4.92 at%. Moreover, the doped graphene synthesized via this method processes better quality and fewer layers than that prepared through many other approaches.

2.2.4 Thermal annealing

Thermal annealing refers to the method utilizing high temperatures to incorporate various dopants into graphene. [108,109] There are usually two approaches. One is to anneal graphene or graphene oxide in dopant-containing gaseous environment. For example, Dai's group [50] developed a facile approach to fabricate a B/N co-doped graphene by thermal annealing GO in the presence of boric acid and ammonia at 1000 ºC. The BCN graphene exhibited superior electrocatalytic abilities to the commercial Pt/C electrocatalyst.

Another approach is the direct pyrolysis of dopant-containing hydrocarbons or polymers in the presence of graphene, which can introduce various atoms to graphene. Ding *et al.* [51] used aniline as precursor to fabricate the doped graphene in layered montmorillonite, a quasi-closed flat nanoreactor, which can selective synthesis of pyridinic- and pyrrolic-nitrogen doped graphene. This method can also realize the co-doping of two or more elements without any side products. Liang *et al.* [52] used melamine and benzyl disulfide (BDS) as N and S precursors respectively, and incorporated them with GO/SiO_2 nanocomposite, in which the SiO_2 spheres were used as the structural template. Finally, N- and S- co-doped graphene was obtained after annealing mixture of melamine/BDS/GO/SiO_2 at high temperature. The properties of the as-prepared doped graphene are highly dependent on the pyrolysis temperatures, and excessively low or high temperature can lead to the low electronic conductivity or a remarkable loss of active sites. The presented N and S dual doped mesoporous graphene can be used as a metal-free catalyst for oxygen reduction with high efficiency. Zheng et al.[104] studied the electronic properties of different heteroatoms (N, B, O, S, P, F) in doped graphene by density functional theory (DFT) calculations. They found that N and O acted as electron acceptors for the adjacent C for their negatively charged. In contrast, F, S, B, and P acted as electron donors for their positively charged. Based on the theoretical prediction, they selected N and P atoms, which were the most noticeable differences in the charge population, to design a dual

doped graphene by annealing chemically exfoliated GO powder with a melamine (N source) and triphenylphosphine (P source) mixture at 950 ºC in Ar atmosphere. The content of dopant was 4.60 atom % of N and 1.63 atom % of P, respectively. With the synergistic effect, the doped graphene was applied to enhance HER, exhibited a significantly improved electrochemical performance.

The shortcoming of the above methods is the relatively high working temperature. The direct thermal annealing process generally results in an irreversible stacking of graphene due to the strong π-interactions. To solve this problem, Yang *et al.* [53] confined GO sheet by a sandwich-like, ultrathin and porous silica shell to facilitate the thermal reaction and prevent the irreversible re-aggregation of grapheme at high temperature, which can achieve nitrogen and sulfur-doped graphene with high surface areas.

2.2.5 Plasma treatment

Plasmon treatment is a facile approach to incorporate foreign atoms and groups into scaffold surfaces. [54] By exposing materials at atmosphere containing doping elements under plasma treatment, the initial atoms can be partly replaced by the foreign atoms. An N-doped graphene was fabricated by the plasma treatment of graphene at nitrogen atmosphere. [11] It was found that the plasma treatment not only introduced nitrogen atoms into the host graphene but also increased the content of oxygen. In this case, the nitrogen content in graphene can be regulated by changing the plasma exposure time. In addition,

Table 1 Synthesis Methods of Doped Graphene and Their Applications.

Synthesis methods	Precursors	Doping elements	Properties	Application
CVD	CH_4/NH_3, Cu film on Si substrate as catalyst	N (1.2-8.9 at%)	N-type semi-conductor, lower conductivity	FET 14
	$NH_3/CH_4/H_2/Ar$ (10:50:65:200), Ni film on SiO_2/Si substrate as catalyst	N (4 at%)	Electrocatalytic activities	ORR 15
	Pyridine, Cu foil as catalyst	N (~2.4 at%)	N-type semi-conductor, Monolayer	FET 16
	Boron powder, Cu foil as catalyst	B (0.5 at%)	P-type semi-conductor, visible transmittance of 95.7%, Hall effect	Solar cells 17
	Methane, boric acid powder, nitrogen gas, Cu foil as catalyst	N (1.38 at %) B (0.62 at %)	P-type semi-conductor	18
	Melamine diborate, nickel foam as catalyst	N (4.5 at %) B (3 at %)	3D, electrocatalytic activities, thermal stabilities	ORR 19
	Graphite oxide, NH_3/Ar	N (2.0-2.8 at%)	N-type semi-conductor, electrocatalytic activities	ORR 20
	GO, NH_3/Ar (10% NH_3)	N (~3-5 at%)	N-type semi-conductor	FET 21
Thermal annealing	Glucose, melamine	N (8.3-29.9 at%)	Electrocatalytic activities	ORR22
	GO, boric acid, NH_3	N B	Electrocatalytic activities	ORR 23
	Thermally exfoliated GO, $(NH_4)_3PO_4$	N (2.9 at%) P (4.3 at%)	high capacitance retention ratio of >80%	Ultracapaci-tor 24
	GO, benzyl disulfide	S (1.3-1.53 at%)	Electrocatalytic activities	ORR 12
	GO, CNT, diphenyl diselenide	Se (1.05 at%)	Electrocatalytic activities	ORR 25
	GO,1-methyl-3-(3-trimethoxysilyl)-propylimidazole chloride	N (1.97-2.40 at%) Si (7.6-5.42 at%)	P-type semi-conductor,low adsorption energy	Gas sensing 26
Solvothermal approach	Li_3N/CCl_4(NG1) or $N_3C_3Cl_3/Li_3N/CCl_4$(NG2)	N (4.5 at% (NG1) or 16.4 at% (NG2))	N-type semi-conductor(NG), p-type semi-conductor (NG2)	ORR 27
	BBr_3, CCl_4, potassium as catalyst	B (0.51 at%)	Electrocatalytic activities P-type semi-conductor	FET 28
Arc discharge method	graphite/H_2/He/pyridine(NG1) or graphite/H_2/He/NH_3(NG2) or transformation of nano-diamond/He/pyridine (NG3) graphite/H_2/He/B_2H_6 (BG1) or boron-packed graphite/H_2/He (BG2)	N (0.6 at% (NG1) or 1 at% (NG2) or 1.4 at% (NG1)) B (1.2 at% (BG1) or 3.1 at% (BG2))		29
Plasma treatment	chemically synthesized graphene, N_2 plasma	N (0.11~1.35 at%)	Electrocatalytic activity	Biosensor 9
	Graphene nanoribbons(GNR), NH_3 plasma	N	N-type semi-conductor	FET 29

Choi's group [55] prepared the N-doped graphene by firstly reducing GO with hydrogen plasma treatment and then N atoms doping was realized by exposing the reduced GO (rGO) with nitrogen plasma. A mild NH_3 plasma-treated graphene doping method was developed by Dai's group. [56] It was demonstrated that the position of the doping atom can be controlled by the plasma treatment conditions, and the mild-plasma caused

doping defects near the edge of a graphene while harsh-plasma damaged the centre of graphene.

With plasmonic effects, metal-based subwavelength antennas injected nonequilibrium hot electrons into nearby graphene structure under resonant illumination and effectively doping the graphene. [57] Hence, Fang *et al.* obtained *n*-type doping graphene by plasmon-generated hot electrons, which can be a good candidate for optoelectronic device and sensors.

There are many other methods to dope graphene with high efficiency. Nicolle *et al.* [58] explored the behaviour of different number of graphene layers supported on SiO_2 under high pressure for a capacitance-induced substrate-mediated charge transfer, which *n*-type doping graphene was fabricated. Kim *et al.* [59] modulated *p*-type doping of graphene by noncovalently latching light switchable dipolar molecules with an hole concentration of ~5×10^{12} cm^{-2}.

3. Properties of doped graphene

Graphene is a zero band gap semiconductor that possesses extraordinary properties such as high mobility of charge carriers, anomalous quantum Hall effect, and superior thermal/electrical conductivity. [60-64] However, the absence of a true band gap is a major drawback for the application in electronic devices (e.g. FETs). Chemical doping not only opens the band gap but also generates specific charge carriers (holes and electrons). [65] Hence, doped graphene has the different properties compared with graphene, showed in Table 2. The incorporation of different heteroatoms into graphene can result in transformation of graphene into *p*- or *n*-type semiconductor respectively, which make the use of graphene nanosheet as a semiconducting channel between the source and drain in FETs possible. [66] We exhibited the doping mechanism in graphene in Fig. 3. Graphene is unique for its zero-gap band structure with the zero density of states (DOS). Chemical doping can induce the desired rigid band. The Fermi level was shifted away from the Dirac point by electrons (or holes), shown as an energy shift in the carbon projected density of states (C-PDOS). Hole (*p*) and electron (*n*) doping can be achieved by contacting the carbon layer with different metals. [67,68] For *n*-type dopants with a HOMO (E_H), the ionization potential I_p decreases as electrons are removed, while charges flow to the graphene from the dopants near the Fermi energy of graphene. For *p*-type dopants with a LUMO (E_L), the electrons affinity increases as electrons are added to the valence level, while charges flow to the dopants from the graphene near the Fermi energy of graphene. [67] Different doping atoms can result in various bond types that have profoundly different effects on the carrier concentration or band gap etc. It has been reported that the *n*-type semiconducting graphene is produced by nitrogen atoms donating its lone pair of electrons to the graphene system network. The lone pair electrons in nitrogen are closely related to high electron mobility. Hence, Some *et al.* [66] selected phosphorus with higher donating ability of lone pair electrons to prepare much stronger *n*-type graphene than nitrogen. Otherwise, the content of dopants also strongly influenced electrochemical activity. Zhang *et al.* [70] found that lower N content can't render enough N-doped graphene electrochemical activity. However, higher N content was able to create more active sites with low conductivity and more sites prone to poisoning. For this reason, suitable N content with acceptable conductivity and considerable active sites is closely related to ORR activity for doped graphene. Meanwhile, Panchakarla *et al.* [71] also reported that the concentration of B and N affected semiconducting electronic properties.

Table 2 The properties of pristine graphene and doped graphene.

	Work Function (eV)	Resistance (Ω/sq)	Visible Transmittance	Hall coefficient (HC, m^2/C)	Ref.
Pristine graphene	4.2	1100	96.7 % (550 nm)		46
Nitric-doped		416	89 %	+26.8	58
Hydrazine-doped		517	89 %	-94.6	58
PEI-doped		397	89 %	-38	58
$AuCl_3$-doped	5.0	500	94.5 % (550 nm)		59
$IrCl_3$-doped	4.9	600	92.5 % (550 nm)		59
$MoCl_3$-doped	4.8	720	86.2 % (550 nm)		59
$RhCl_3$-doped	5.14	620	~90 % (550 nm)		59

The dopants also play an important role in magnetoresistance (MR). Rein *et al.* [105] clarified the influence of nitrogen doping on magnetotransport of single layer graphene by CVD. Compared to undoped graphene, there was a 6-fold increase in the charge carrier concentration up to 4×10^{13} cm^{-2} for doped graphene at room temperature. Meanwhile, due to the Lorentz MR, a positive high filed MR was found on graphene. In contrast, a negative MR is observed for doped graphene at both 2.3K and 279 K, which was ascribed to the defect boundary scattering, leading to reverses MR.

It has been known that the energy level is different between graphene electrode and other active layers, which prevented the application of graphene in light emitting diodes, organic light emitting diodes, or organic solar cells. This problem can be solved by modulation of work function in the graphene layer with doping high work function metals. Kwon *et al.* [72] investigated six metal chlorides as the *p*-type dopants to tune work function of graphene. The results were listed in Table 3. It can be concluded from Table 3 that graphene doped by metal chlorides can greatly decrease its sheet resistance and transmittance. They found that $RhCl_3$ was the strongest *p*-dopant due to the highest work function.

Table 3 Electronic properties of doped graphene.

	Pristine graphene	Doped graphene	Heteroatoms	Application	Ref
Carrier mobility ($cm^2V^{-1}s^{-1}$)	2×10^5	Up to11.5&12.4 (hole & electron)	N	FET	74
Dirac point (V)	0	-16	N	FET	74
Resistance (Ω)	10^3	$10^2 \sim 10^8$	N	ORR	45
Raman scattering		10 times than graphene	N	molecule sensing	76

Similar to electronic properties, the optical properties of graphene can also be tuned by chemical doping. Bult *et al.* [69] demonstrated chemically doped *p*-type and *n*-type graphene transparent conducting electrodes that possess 89% visible transmittance, which are well-suited as anodes or cathodes for a variety of opto-electronic applications. It's also reported the photoluminescence of rGO can be quenched by doping. [73] Meanwhile, UV-vis absorption spectrum of N-doped graphene quantum dots (N-GODs) showed blue-shifted and emitted intense blue luminescence. [74,75] In addition, N-doped graphene can also enhance Raman of RhB molecules. [76]

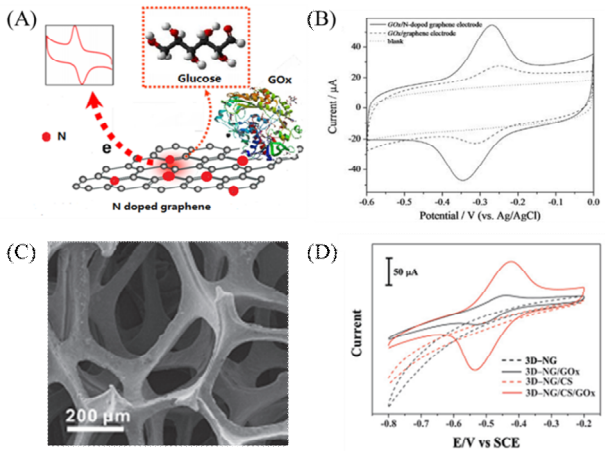

Fig. 6 (A) Scheme of detection of glucose by N doped graphene and graphene. (B) Cyclic voltammograms of GOx immobilized on N-doped graphene electrode (solid line), graphene electrode (dashed line) and GCE (dotted line) in N_2-saturated 0.1 M PBS solution (pH 7.0). Scan rate = 0.05 V s^{-1}. (C) SEM images of 3D-NG. (D) Cyclic voltammograms of bare 3D-NG (black dashed curve), 3D-NG/GOx (black curve), 3D-NG/CS (red dashed curve) and 3D-NG/CS/GOx (red curve) in N_2-saturated 0.1 M PBS (pH = 7.40). Scan rate = 0.1 V s^{-1}. [a] Reprinted with permission from ref. 11, Copyrights (2010) American Chemical Society and from ref. 83, Copyrights (2015) Royal Society of Chemistry, respectively.
[a] Abbreviation: Chitosan (CS)

4. Applications in Bioanalysis

Compared to pristine graphene, the results indicate that the unoccupied DOS changes after doping, suggesting charge transfer between carbons to the dopants, which is beneficial for the electric conductivity of the materials. [77] Secondly, doping can alter the surface oxygen-containing groups on graphene to improve the resistance of graphene further. Thirdly, doped graphene increases specific surface area, which is easier to decorate molecules on it. Moreover, doping introduces more defects to the graphene, resulting in more catalytic sites to enhance the catalytic properties of graphene towards molecules. [78,79] Hence, doped graphene has attracted an enormous amount of interest in bioanalysis applications. According to the analytical targets, we discussed the application in the following aspects, including small molecules, proteins and cells sensor.

4.1 Small molecules sensor

Hydrogen peroxide (H_2O_2) is important in regulator of eukaryotic signal transduction and response to various stimuli including cytokines and growth factors, which is also an essential mediator in food, industrial, and environmental analysis. [80,81] Shao *et al.* [82] introduced a facile method to produce N-graphene by exposing functionalized graphene sheet (FGS) in nitrogen plasma. The carbon atoms adjacent to nitrogen dopants possessed a higher positive charge density in doped graphene, which enhanced adsorption of H_2O_2. Meanwhile, the nitrogen-induced charge delocalization changed the chemisorption of O_2 from monoatomic end-on adsorption to diatomic side-on adsorption, which effectively weakened the O–O bond to facilitate electrocatalytic reduction of H_2O_2. Furthermore, N elements in graphene also created some structural defects on graphene with an amount of unsaturated carbon atoms, which are very active to react with H_2O_2. Hence, N-graphene exhibited greatly electrocatalytic activity toward H_2O_2 reduction. A well-defined reduction peak around -0.2 V in the CV on N-graphene with a linear relationship from 10^{-5} mM to 2.8 mM, which was much wider than that on graphene (10^{-4} mM to1.8 mM). As H_2O_2 is a general enzymatic product of glucose, it is supposed that doped graphene improve the catalytic activity to glucose, which is the diabetes target analyte. However, other than H_2O_2, the catalytic site of glucose oxidase is seated deeply in a cavity and not easily accessible, which limits catalytic activity of glucose oxidase. The doped graphene produced by Wang *et al.* [11] displayed good biocompatibility, high electrocatalytic activity and fast direct electron transfer kinetics for enzymes, realizing glucose biosensing with high sensitivity. As showed in Fig. 6A, they obtained N-doped graphene by nitrogen plasma treatment of graphene with regulating N percent in host graphene from 0.11-1.35%. The nitrogen atom was inset into the graphite plane to form quaternary N or graphitic nitrogen (G-N), while nitrogen atoms were doped in graphene to form pyridinic N and pyrrolic N. Due to the change of the density of electronic states (DOES) by doping effects, the functional graphene had better performance in electrocatalysis. More importantly, the N doped graphene showed remarkable ability for electron transfer from

the enzyme cavity to the electrode surface, resulting in good response for glucose from 0.01 to 0.5 mM in the presence of interferences (Fig. 6B). As electron transfer is sensitive to the surface chemistry and DOES near the Fermi potential, the redox peak current is much higher on N-doped graphene than on graphene. Due to the porous structures that may offer higher surface area for enzyme loading, Guo *et al.* [83] proposed a new kind of enzyme carrier for biosensors by three-dimensional (3D) network. They utilized chemical vapour deposition to prepare a highly conductive 3D nitrogen doped graphene (3D-NG) structure, show in Fig. 6C, 6D, which exhibited higher redox peak currents than 3D graphene. The sensitivities of the 3D-NG sensor for glucose were 226.24 μA mM^{-1} cm^{-2} for the lower concentration region and 108.94 μA mM^{-1} cm^{-2} for the higher concentration region. This was ascribed to the hydrogen bonds of nitrogen-containing groups in 3D-NG, which can promote the adsorption of biomaterials. Moreover, by calculating the surface coverage concentration of the electroactive glucose oxidase (GOx), it's concluded that the 3D porous structure provided more specific surface area and adsorption sites for enzyme loading.

Ascorbic acid (AA), uric acid (UA) and dopamine (DA) are closely related to physiological function of organisms and many diseases including cancer, Parkinson's disease and cardiovascular disease. [82] However, AA, DA and UA usually coexist and their oxidation potentials are severely overlapped, which make them selective detection difficult. Sheng *et al.* [84] developed a facile approach to synthesize nitrogen doped graphene by thermally annealing a mixture of GO and melamine. The nitrogen doped graphene realized to detect AA, DA and UA simultaneously with high sensitivity. The linear ranges are 5.0×10^{-6} to $1.3.0\times10^{-3}$ M, 5.0×10^{-7} to 1.7×10^{-4} M and 1.0×10^{-7} to 2.0×10^{-5} M with detection limit of 2.2×10^{-6} M, 2.5×10^{-7} M and 4.5×10^{-8} M (S/N = 3) for AA, DA and UA respectively. The highly electrocatalytic activity of the sensor was related to the fact that nitrogen atoms in NG layers may interact with these molecules via hydrogen bond, which can activate the hydroxyl and amine groups, and further accelerate the charge transfer kinetics of these molecules at NG surface. Meanwhile, the π-π interactions between graphene layers and these molecules can also promote the charge transfer of the three molecules. The selective analysis of DA in the presence of AA and UA were also realized on the boron doped graphene modified electrode. [85] In addition, the boron doped graphene also exhibited electrochemical activity toward the oxidization of β-nicotinamide adenine dinucleotide (NADH), which is of great interest since it is required in a whole diversity of dehydrogenase-based biosensors. [86] Importantly, the boron doped graphene modified electrode showed excellent performance towards NADH oxidation product fouling. The boron atoms in graphene decreased the electron density of neighbour carbon sites, which had an impact on the chemical and electrochemical activity of boron doped graphene to biomolecules.

NO_2^- is also an important anion which has been recognized as an alarming pollutant to the environment and human health. Excessive NO_2^- in human body may cause methemoglobinemia and may become source of carcinogenic N-nitrosamines. [87,88] By the π-stacking interaction between graphene and phenanthrene, Li *et al.* [89] added graphene to phenanthrene/K solution complex to prepare K doped graphene, which showed a high response toward the oxidation of NO_2^-. Based on the K doped graphene sensing platform, a detection limit of 0.2 μM was obtained at a signal-to-noise ratio of 3 with the linear ranging from 0.5 μM to 7.8 mM. The sensor also successfully applied to determinate NO_2^- released from liver cancer and leukemia cells, showing a good potential in biomedical application. As the different types of K species (mainly K oxides, K ions, and K metal) in graphene, it might introduce a change in the Fermi level and charge transfer of the graphene. As a consequence, K modification might be beneficial to regulate the electronic properties and enhancing the electrocatalytic activity of graphene in electrochemical systems. This method can be extended to the chemical modification of other alkali metals, which enable the formation of the most variations of graphene.

As metal nanoparticles have a large specific active surface area, they can be distributed on the graphene as tiny conducting centres. Hence, the incorporation of metal nanoparticle into graphene can decrease the energy barrier, enhance electron transfer and improve biosensor response. [78,110] In this regard, Kannan *et al.* [78] introduced platinum nanoparticle into nitrogen doped graphene (N-GN-PtNP) to detect the homocysteine with experimental detection limit of 200 pM. It was showed that the potential shifted to 210 mV positively and the oxidation current improved 3-fold higher on N-GN-PtNP modified electrode. It was also implied by authors that nitrogen atoms facilitate the interaction between graphene and metals, which can improve the biosensing efficiency further.

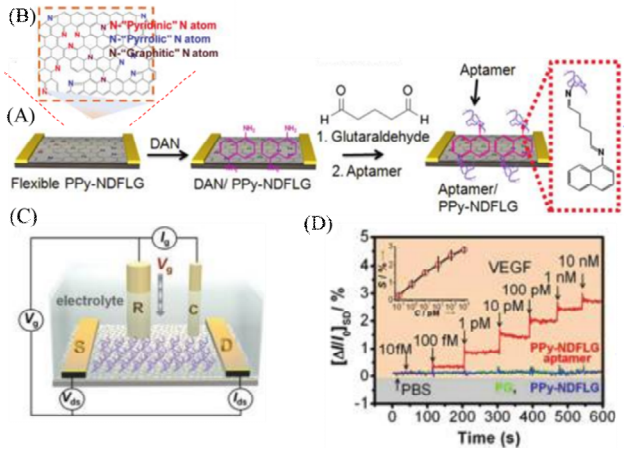

Fig. 7 (A) Schematic illustration of reaction steps for the fabrication of aptasensor platforms based on PPy-NDFLG conjugated with anti-VEGF RNA aptamer. (B) Structure diagram of PPy-NDFLG. (C) Schematic diagram of a liquid-ion gated FET using aptamer conjugated PPy-NDFLG. (D) Real-time responses and a calibration curve of aptasensor with various vascular endothelial growth factor concentrations. Reprinted with permission from ref. 10, Copyrights (2012) American Chemical Society.

4.2 Protein sensors

Proteins are vital for gene expression mechanisms and reflect the development of diagnostics for disease states. Due to the excellent properties of graphene, such as ambipolar electric field effect and high carrier mobility, Graphene-based FETs are considered to be the most promising replacement to the silicon electronics. However, a zero-gap and ambipolar characteristic are limited the application of graphene in electronics. Doping can solve these problems by injecting or extracting carrier to tailor the electronic structure, thus tuning band gap. Jang's group [10] applied doped graphene in FET device to detect biomolecules with high sensitivity. They grew nitrogen doped few-layer graphene (PPy-

NDFLG) by polypyrrole as the solid source with CVD method. After nitrogen doping, there were three kinds of N atoms in functional graphene with exhibiting stable *n*-type behaviour, shown in Fig. 7B. They utilized PPy-NDFLG as a signal transducer and integrated with an anti-VEGF RNA aptamer into a flexible FET platform to detect vascular endothelial growth factor (VEGF), which is the useful for the early diagnosis, staging and monitoring of cancers (Fig. 7C). It was shown in Fig. 7A that anti-VEGF RNA aptamer was performed by modifying the plane of PPy-NDFLG with glutaraldehydeconjugated 1,5-diaminonaphthalene (DAN) through a Schiff-base reaction. [90-94] As the interactions between aptamer and VEGF affected the charge-carrier density on the surface of PPy-NDFLG, the electronic control was realized. This concentration-dependent sensor gave a rapid response time of less than 1s with a detection limit of 100 fM, which were approximately 1-3 orders lower than that of conventional VEGF sensors (Fig. 7D). Moreover, the FET-type aptasensor displayed outstanding mechanical flexibility suitable for fabrication portable and implantable sensors.

For biological recognition events, electrochemiluminescence (ECL) technique is a versatile method with low background signal, desirable sensitivity and good analytical performance. In ECL process, the key factor to affect the signal is the electron transfer reaction between formed nanocrystal species and co-reactants. To enhance the signal, the nanocrystals hold great promise for its potential applications with remarkable electronic activities, chemical stability, and large surface area. Wang *et al.* [95] developed metal K doped graphene with SiO_2@CdS nanocomposites to fabricate a sensitive ECL sensor successfully (Fig. 8). They found that the doped K in graphene with three species K cations, K oxides and K metal, not only accelerated the electron transfer in the ECL reaction, but also anchored more SiO_2@CdS/DNA composites due to its high surface/volume ratio. They applied this sensor to detect the ubiquitous transcriptional factor TATA-binding protein (TBP). The detection limit of TBP in this work was found at levels down to 0.02 nM, which was superior to that obtained from electrochemical assay (3 nM). To improve ECL efficiency and stability of luminophores, Wang's group [104] involved silver bromide nanoparticles (AgBr NPs) on nitrogen doped graphene by the water bath method. The $AgBr^{\bullet}$ released an electron, which from the oxidizing agent $SO_4^{\bullet-}$ radicals, to form the AgBr* for ECL emission. In this system, nitrogen doped graphene worked as an electron reservoir to accept the electron from the CB of *n*-type AgBr, which can avoid that Ag^+ captured the photogenerated electrons.

In order to acquire more chemically active sites, further functionalization on doped graphene can carry out to achieve better electrochemical performances. Generally, there are some functional groups such as CN, NH_3 or SH in the proteins, the active groups are easy to coordinate with metals, which can not only increase the surface area of the nanocomposites but also improve the capture amounts of proteins. Matrix metalloproteinase-2 (MMP-2), a protease related to tumor growth, invasion, reproduction and tissue remodeling, is secreted by malignant tumor cells. It is of great importance to analyze MMP-2 sensitively in the early detection of disease. In this regard, Zhu's group [96] involved Au nanoparticles on nitrogen doped graphene network to fabricate an ultrasensitive electrochemical immunosensor to detect MMP-2. It was demonstrated that the hydrophobicity and hence biocompatibility were improved by incorporation Au on doped graphene, more suitable for proteins loading. Consequently, the immunosensor showed linear detection, ranging from 0.0005 to 50 ng mL^{-1} with a detection limit of 0.11 pg mL^{-1}. The detection limit of precious reports was 0.02 ng mL^{-1}, much higher than this proposed system.

The doped graphene composites were also employed to the fabrication of non-mediator electrochemical biosensor for several of biomarkers detection, such as alpha-fetoprotein (AFP) [97] and zearalenone. [98] To produce higher catalytic efficiency, Ju's group [99] assembled of hemin on N-doped graphene (hemin@NG) to quench the ECL emission of QDs by electrocatalytically reducing the dissolved oxygen, the ECL coreactant. Due to the doping of nitrogen, the N atoms as the electron donors to promote the reactivity of adsorbed molecules. Meanwhile, hemin is normally used as an HRP mimic, owing its capability as oxygen reduction catalyst. The N defective sites on graphene can coordinate with the iron active centre in hemin for better immobilization, which can facilitate the electrocatalytic reduction. This new ultrasensitive immunoassay sensor was used to detect carcinoembryonic antigen (CEA), showing a detection limit of subpicogram per milliliter with the linear range over five orders of magnitude.

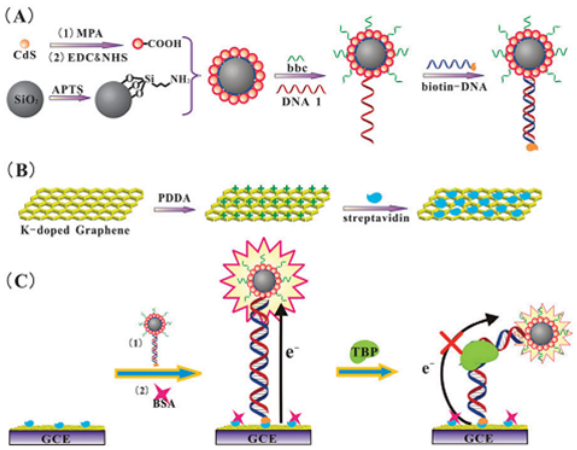

Fig. 8 The analytical procedure of the amplified ECL TBP assay. Reprinted with permission from ref. 95, Copyrights (2010) Royal Society of Chemistry.

4.3 Cell sensors

Due to the growth, metabolism and apoptosis of cells are closely related to biological environments in organisms, it's of great significance to visualize and monitor physiological events to understand cell biology. The physiological processes or diseases are related to special biomolecules, which served as biomarkers. By introducing probes, these biomarkers can be traced to reveal the activities of living cells in molecular level, especially for tumors. Thus, it plays an important role in discovery and treatment of diseases. With non-invasiveness and high sensitivity, fluorescent spectroscopic techniques offer excellent observation for intracellular signaling and intracellular analysis.

Two-photon fluorescence imaging (TPFI) is suitable for cell in vivo bioimaging because of larger penetration depth, minimized tissue autofluorescence background and photodamage in biotissues. The two-photonfluorescent probes with enough brightness are essential for scattering deep tissues. With bleaching, low cytotoxicity and excellent biocompatibility, graphene quantum dot (GQD) is one of the most ideal options for two-photonfluorescent probes. After nitrogen doping, it can be introduced strong electron-donating groups (such as dimethylamido) to GQD. The lone pair electrons from dimethylamido formed the *p*-π conjugation with the aromatic

rings to enlarge the π-conjugated system. The primary HOMO was elevated to a higher energy obit by the strong orbital interaction, further decrease of bandgap and redshift of fluorescence emission. Furthermore, the large π-conjugated system facilitated the charge transfer efficiency and enhanced the two-photon absorption, which provided strong two-photon-induced fluorescence for N-GQD. Gong [75] used N-GOD as two-photon fluorescent probes for cellular and deep-tissue imaging. As is shown in Fig. 9A, the lone pair electrons from donating group dimethylamido were doped to the plane of N-GOD, which can enlarge the π-conjugated system. The primary HOMO (blue dashed line in Fig. 9A) was promoted to a higher energy obit HOMO (black solid line) by the orbital interaction between dimethylamido and π-conjugated system of N-GOD. Then, the bandgap decreased and fluorescence emission was red-shift. Furthermore, dimethylamido and π-conjugated system of N-GOD can facilitate the charge transfer efficiency and the two-photon absorption. They used DMF as the source of nitrogen and GO as the carbon source to fabricated N-GQD. N-GQD showed a two-photon absorption cross section as high as 48000 GM and a large imaging penetration depth of 1800 μm (Fig. 9B, 9C).

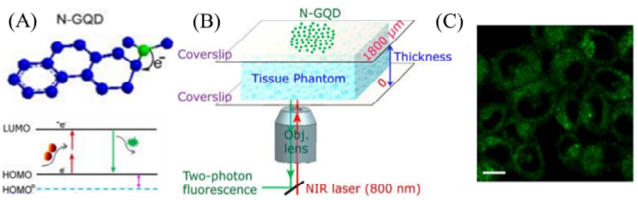

Fig. 9 (A) Fluorescence mechanism of N-GQD. (B) Schematic of the setup used for TPFI of N-GQDs in tissue phantom with different thickness. (C) Two-photo cell imaging under 800 nm excitation. Reprinted with permission from ref. 75, Copyrights (2013) American Chemical Society.

Considering the excellent properties of carbon nanomaterials in the biosensing applications, the doped carbon nanomaterials have drawn much attention in the cell imaging application due to their high quantum efficiency and biocompatibility. For example, Si-doped carbon quantum dots [100] and nitrogen-doped carbonaceous nanospheres [101] have been successfully applied for bioimaging in cell. However, it is still an initial stage for the carbon nanomaterials in the applications of fluorescent chemosensors to monitor and image biological processes. It is anticipated that the doped graphene possesses brilliant future in monitoring biological activity of deep tissues and detecting the disease of living biosystems.

5. Conclusion and perspective

In summary, we represent an overview of the recent development in doped graphene. Various synthesis methods have been reported to obtain heteroatoms doped graphene with tuned band gap. Endowed with a real band gap, it can be used as *p*-type or *n*-type semiconductor. Compared to pristine graphene, both physical and chemical properties of doped graphene can be tailored. The dopants changed the electron density of neighbouring carbon atoms, which determined its physical properties such as electrical conductivity and transparency. Meanwhile, dopants can act as active sites for catalysis in electrochemical sensors. In the future work, key insights into the doping mechanism such as the bonding type, the dopant location and the influence factors of doping should be further explored.

Besides the applications of doped graphene in energy related areas, the extraordinary properties make it a promising material for bioanalysis. The increased active sites caused by heteroatoms show excellent activity towards small molecules. In addition, doped graphene endowed with a real band gap is an ideal material for FET and ECL, which improve the detection limit for proteins or cells by several orders of magnitude. We believe there will be more doped graphene based methods developed for biomolecules detection in the future.

Acknowledgements

This work was financially supported by National Basic Research Program of China (No. 2011CB935704, No. 2013CB934004), the National Natural Science Foundation of China (No. 21375073, No. 21235004, 21327806, No. 11079002), Research Fund of Ministry of Education of China (No. 20110002130007) and Tsinghua University Initiative Scientific Research Program (NO. 2014z21027).

References

1. K. S. Novoselov, A. K. Geim, S. V. Morozov, D. Jiang, Y. Zhang, S. and V. Dubonos, *Science*, 2004, **306**, 666.
2. X. Huang, X. Qi, F. Boey and H. Zhang, *Chem. Soc. Rev.*, 2012, **41**, 666.
3. M. D. Stoller, S. Park, Y. Zhu, J. An and R. S. Ruoff, *Nano Lett*, 2008, **8**, 3498.
4. C. Cheng, S. Li, S. Nie, W. Zhao, H. Yang, S. Sun and C. Zhao, *Biomacromolecules*, 2012, **13**, 4236.
5. C. Cheng, S. Nie, S. Li, H. Peng, H. Yang, L. Ma, S. Sun and C. Zhao, *J. Mater. Chem. B*, 2013, **1**, 265.
6. H. Liu, Y. Liu and D. Zhu, *J. Mater. Chem.*, 2011, **21**, 3335.
7. A. H. Castro Neto, F. Guinea, N. M. R. Peres, K. S. Novoselov, and A. K. Geim, *Rev. Mod. Phys.*, 2009, **81**, 109.
8. I. Gierz, C. Riedl, U. Starke, C. R. Ast and K. Kern, *Nano Lett.*, 2008, **8**, 4603.
9. D. Wei and Y. Liu, *Adv. Mater.*, 2010, 22, 3225.
10. O. S. Kwon, S. J. Park, J. Y. Hong, A. R. Han, J. S. Lee, J. S. Lee, J. H. Oh and J. Jang, *ACS Nano*, 2012, **6**, 1486.
11. Y. Wang, Y. Shao, D. W. Matson, J. Li and Y. Lin, *ACS Nano*, 2010, **4**, 1790.
12. A. J. Samuels and J. D. Carey, ACS Nano, 2013, **7**, 2790.
13. T. O. Wehling, K. S. Novoselov, S. V. Morozov, E. E. Vdovin, M. I. Katsnelson and A. K. Geim, *Nano Lett.*, 2008, **8**, 173.
14. P. Wei, N. Liu, H. R. Lee, E. Adijanto, L. Ci and B. D. Naab, *Nano Lett.*, 2013, 13, 1890.
15. F. Yavari, C. Kritzinger, C. Gaire, L. Song, H. Gulapalli and T. Borca-Tasciuc, *Small*, 2010, **6**, 2535.
16. F. Schedin, A. K. Geim, S. V. Morozov, E. W. Hill, P. Blake and M. I. Katsnelson, *Nat. Mater.*, 2007, **6**, 652.
17. N. Jung, N. Kim, S. Jockusch, N. J. Turro, P. Kim and L. Brus, *Nano Lett.*, 2009, **9**, 4133.
18. S. Some, J. Kim, K. Lee, A. Kulkarni, Y. Yoon and S. Lee, *Adv. Mater.* 2012, **24**, 5481.
19. W. Chen, S. Chen, D. Qi, X. Gao, and A. T. Wee, *J. Am. Chem. Soc.*, 2007, **129**, 10418.
20. Y. H. Lu, W. Chen and Y. P. Feng, *J. Phys. Chem. B*, 2009, **113**, 2.
21. X. Dong, D. Fu, W. Fang, Y. Shi, P. Chen and L. J. Li., *Small*, 2009, **5**, 1422.
22. D. B. Farmer, R. Golizadeh-Mojarad, V. Perebeinos, Y. M. Lin, G. S. Tulevski, J. C. Tsang, *Nano Lett.*, 2009, **9**, 388.
23. P. Wei, N. Liu, H. R. Lee, E. Adijanto, L. Ci and B. D. Naab, *Nano Lett.*, 2013, **13**, 1890.
24. G. Giovannetti, P. Khomyakov, G. Brocks, V. Karpan and J. Brink, P. Kelly, *Phys. Rev. Lett.*, 2008, **101**, 026803.
25. H. Wang, T. Maiyalagan and X. Wang, ACS Catal., 2012, 2, 781.
26. Y. Zhang, L. Zhang and C. Zhou, *Acc. Chem. Res.*, 2013, **46**, 2329.
27. T. Kato and R. Hatakeyama, *ACS Nano*, 2012, **6**, 8508.

28. Y. Xue, B. Wu, L. Jiang, Y. Guo, L. Huang and J. Chen, *J. Am. Chem. Soc.*, 2012, **134**, 11060.
29. K. Yan, L. Fu, H. Peng, Z. Liu, *Acc. Chem. Res.*, 2013, **46**, 2263.
30. X. Li, W. Cai, L. Colombo, R. S. Ruoff, *Nano Lett.*, 2009, **9**, 4268.
31. A. Reina, S. Thiele, X. Jia, S. Bhaviripudi, M. S. Dresselhaus and J. A. Schaefer, *Nano Res.*, 2009, **2**, 509.
32. B. Dai, L. Fu, Z. Zou, M. Wang, H. Xu and S. Wang, *Nat. Comm.*, 2011, **2**.
33. N. Liu, L. Fu, B. Dai, K. Yan, X. Liu, R. Zhao, Y. Zhang and Z. Liu, *Nano Lett.*, 2011, **11**, 297.
34. X. Liu, L. Fu, N. Liu, T. Gao, Y. Zhang, L. Liao and Z. Liu, *J. Phys. Chem. C*, 2011, **115**, 11976.
35. Y. F. Lu, S. T. Lo, J. C. Lin, W. Zhang, J.-Y. Lu, F. H. Liu, C. M. Tseng, Y. H. Lee, C. T. Liang and L. J. Li, *ACS Nano*, 2013, **7**, 6522.
36. H. Wang, Y. Zhou, D. Wu, L. Liao, S. Zhao, H. Peng and Z. Liu, *Small*, 2013, **9**, 1316.
37. A. L. M. Reddy, A. Srivastava, S. R. Gowda, H. Gullapalli, M. Dubey and P. M. Ajayan, *ACS Nano*, 2010, **4**, 6337.
38. Z. Jin, J. Yao, C. Kittrell and J. M. Tour, ACS Nano, 2011, 5, 4112.
39. P. C. Chang, Z. Y. Fan, D. W. Wang, W. Y. Tseng, W. A. Chiou, J. Hong and J. G. Lu, *Chem. Mater.*, 2004, **16**, 5133.
40. H. M. Jeong, J. W. Lee, W. H. Shin, Y. J. Choi, H. J. Shin, J. K. Kang and J. W. Choi, *Nano Lett.*, 2011, 11, 2472.
41. X. Li, L. Fan, Z. Li, K. Wang, M. Zhong, J. Wei, D. Wu and H. Zhu, *Adv. Energy Mater.*, 2012, **2**, 425.
42. H. Liping, W. Bin, C. Jianyi, X. Yunzhou, G. Dechao, G. Yunlong, Y. Gui and L. Yunqi, *Small*, 2013, **9**, 1330.
43. J. Han, L. L. Zhang, S. Lee, J. Oh, K.-S. Lee, J. R. Potts, J. Ji, X. Zhao, R. S. Ruoff and S. Park, *ACS Nano*, 2013, **7**, 19.
44. D. Deng, X. Pan, L. Yu, Y. Cui, Y. Jiang, J. Qi, W.-X. Li, Q. Fu, X. Ma, Q. Xue, G. Sun and X. Bao, *Chem. Mater.*, 2011, **23**, 1188.
45. Z. S. Wu, A. Winter, L. Chen, Y. Sun, A. Turchanin, X. Feng and K. Muellen, *Adv. Mater.*, 2012, **24**, 5130.
46. O. Volotskova, I. Levchenko, A. Shashurin, Y. Raitses, K. Ostrikov and M. Keidar, *Nanoscale*, 2010, **2**, 2281.
47. B. Shen, J. Chen, X. Yan and Q. Xue, *RSC Adv.*, 2012, **2**, 6761.
48. L. S. Panchokarla, K. S. Subrahmanyam, S. K. Saha, A. Govindaraj, H. R. Krishnamurthy, U. V. Waghmare and C. N. R. Rao, *Adv. Mater.*, 2009, **21**, 4726.
49. L. Huang, B. Wu, J. Chen, Y. Xue, D. Geng, Y. Guo, G. Yu and Y. Liu, *Small*, 2013, **9**, 1330.
50. S. Wang, L. Zhang, Z. Xia, A. Roy, D. W. Chang, J. B. Baek and L. Dai, *Angew. Chem. Int. Ed.*, 2012, **51**, 4209.
51. W. Ding, Z. Wei, S. Chen, X. Qi, T. Yang, J. Hu, D. Wang, L. J. Wan, S. F. Alvi and L. Li, *Angew. Chem. Int. Ed.*, 2013, **52**, 11755.
52. J. Liang, Y. Jiao, M. Jaroniec and S. Z. Qiao, *Angew. Chem. Int. Ed.*, 2012, **51**, 11496.
53. S. Yang, L. Zhi, K. Tang, X. Feng, J. Maier and K. Muellen, *Adv. Funct. Mater.*, 2012, **22**, 3634.
54. Q. D. Chen, L. M. Dai, M. Gao, S. M. Huang and A. Mau, *J. Phys. Chem. B*, 2001, **105**, 618.
55. H. M. Jeong, J. W. Lee, W. H. Shin, Y. J. Choi, H. J. Shin, J. K. Kang and J. W. Choi, *Nano Lett.*, 2011, **11**, 2472.
56. T. Kato, L. Jiao, X. Wang, H. Wang, X. Li, L. Zhang, R. Hatakeyama and H. Dai, *Small*, 2011, **7**, 574.
57. Z. Fang, Y. Wang, Z. Liu, A. Schlather, P. M. Ajayan, F. H. L. Koppens, P. Nordlander and N. J. Halas, *ACS Nano*, 2012, **6**, 10222.
58. J. Nicolle, D. Machon, P. Poncharal, O. Pierre-Louis and A. San-Miguel, *Nano Lett.*, 2011, **11**, 3564.
59. M. Kim, N. S. Safron, C. Huang, M. S. Arnold and P. Gopalan, *Nano Lett.*, 2012, **12**, 182.
60. C. K. Chang, S. Kataria, C. C. Kuo, A. Ganguly, B. Y. Wang, J. Y. Hwang, K. J. Huang, W. H. Yang, S. B. Wang, C. H. Chuang, M. Chen, C. I. Huang, W. F. Pong, K. J. Song, S. J. Chang, J. H. Guo, Y. Tai, M. Tsujimoto, S. Isoda, C. W. Chen, L. C. Chen and K. H. Chen, *ACS Nano*, 2013, **7**, 1333.
61. K. S. Novoselov, A. K. Geim, S. V. Morozov, D. Jiang, M. I. Katsnelson, I. V. Grigorieva, S. V. Dubonos and A. A. Firsov, *Nature*, 2005, **438**, 197.
62. R. Cheng, J. Bai, L. Liao, H. Zhou, Y. Chen, L. Liu, Y.-C. Lin, S. Jiang, Y. Huang and X. Duan, *Proc. Natl. Acad. Sci. U. S. A*, 2012, **109**, 11588.
63. Y. Wu, K. A. Jenkins, A. Valdes-Garcia, D. B. Farmer, Y. Zhu, A. A. Bol, C. Dimitrakopoulos, W. Zhu, F. Xia, P. Avouris and Y. M. Lin, *Nano Lett.*, 2012, **12**, 3062.
64. F. Bonaccorso, Z. Sun, T. Hasan and A. C. Ferrari, Nat. Photonics, 2010, 4, 611.
65. D. W. Chang, E. K. Lee, E. Y. Park, H. Yu, H. J. Choi, I. Y. Jeon, G. J. Sohn, D. Shin, N. Park, J. H. Oh, L. Dai and J. B. Baek, *J. Am. Chem. Soc.*, 2013, **135**, 8981.
66. S. Some, J. Kim, K. Lee, A. Kulkarni, Y. Yoon, S. Lee, T. Kim and H. Lee, *Adv. Mater.*, 2012, **24**, 5481.
67. G. Giovannetti, P. A. Khomyakov, G. Brocks, V. M. Karpan, J. van den Brink and P. J. Kelly, *Phys. Rev. Lett.*, 2008, **101**, 026803
68. P. A. Khomyakov, A. A. Starikov, G. Brocks and P. J. Kelly, *Phys. Rev. B*, 2010, **82**, 115437
69. R. A. Nistor, D. M. Newns and G. J. Martyna, *ACS Nano*, 2011, **5**, 3096.
70. Y. Zhang, J. Ge, L. Wang, D. Wang, F. Ding, X. Tao and W. Chen, *Sci. Rep.*, 2013, **3**, 2771,
71. L. S. Panchakarla, K. S. Subrahmanyam, S. K. Saha, A. Govindaraj, H. R. Krishnamurthy, U. V. Waghmare and C. N. R. Rao, *Adv. Mater.*, 2009, **21**, 4726.
72. K. C. Kwon, K. S. Choi and S. Y. Kim, *Adv. Funct. Mater.*, 2012, **22**, 4724.
73. M. Li, Z. Wu, W. Ren, H. Cheng, N. Tang, W. Wu, W. Zhong and Y. Du, *Carbon*, 2012, **50**, 5286.
74. Y. Li, Y. Zhao, H. Cheng, Y. Hu, G. Shi, L. Dai and L. Qu, *J. Am. Chem. Soc.*, 2012, **134**, 15.
75. Q. Liu, B. Guo, Z. Rao, B. Zhang and J. R. Gong, *Nano Lett.*, 2013, **13**, 2436.
76. R. Lv, Q. Li, A. R. Botello-Mendez, T. Hayashi, B. Wang, A. Berkdemir, Q. Hao, A. L. Elias, R. Cruz-Silva, H. R. Gutierrez, Y. A. Kim, H. Muramatsu, J. Zhu, M. Endo, H. Terrones, J. C. Charlier, M. Pan and M. Terrones, *Sci. Rep.*, 2012, **2**, 586,
77. D. Geng, S. Yang, Y. Zhang, J. Yang, J. Liu, R. Li, T. K. Sham, X. Sun, S. Ye and S. Knights, *Appl. Surf. Sci.*, 2011, **257**, 9193.
78. P. Kannan, T. Maiyalagan, N. G. Sahoo and M. Opallo, *J. Mater. Chem. B*, 2013, **1**, 4655.
79. D. Usachov, O. Vilkov, A. Grueneis, D. Haberer, A. Fedorov, V. K. Adamchuk, A. B. Preobrajenski, P. Dudin, A. Barinov, M. Oehzelt, C. Laubschat and D. V. Vyalikh, *Nano Lett.*, 2011, **11**, 5401.
80. J. Wang, *Electroanalysis*, 2005, **17**, 7.
81. M. Zhou, Y. M. Zhai, S. J. Dong, *Anal. Chem.*, 2009, **81**, 5603
82. Y. Shao, S. Zhang, M. H. Engelhard, G. Li, G. Shao, Y. Wang, J. Liu, I. A. Aksay and Y. Lin, *J. Mater. Chem.*, 2010, , 7491.
83. J. Guo, T. Zhang, C. Hu and L. Fu, *Nanoscale*, 2015, **7**, 1290.
84. Z. H. Sheng, X. Q. Zheng, J. Y. Xu, W. J. Bao, F. B. Wang and X. H. Xia, *Biosens. Bioelectron.*, 2012, **34**, 125.
85. S. M. Tan, H. L. Poh, Z. Sofer and M. Pumera, *Analyst*, 2013, **138**, 4885.
86. L. Tang, Y. Wang, Y. Li, H. Feng, J. Lu and J. Li, *Adv. Funct. Mater.*, 2009, **19**, 2782.
87. P. Wang, Z. Mai, Z. Dai, Y. Li and X. Zou, *Biosens. Bioelectron.*, 2009, **24**, 3242.
88. S. S. Mirvish, *Cancer Lett.*, 1995, **93**, 17
89. X. R. Li, F. Y. Kong, J. Liu, T. M. Liang, J. J. Xu and H. Y. Chen, *Adv. Funct. Mater.*, 2012, **22**, 1981.
90. X. Dong, Y. Shi, W. Huang, P. Chen and L. J. Li, *Adv. Mater.*, 2010, **22**, 1649.
91. B. Gulbakan, E. Yasun, M. I. Shukoor, Z. Zhu, M. You, X. Tan, H. Sanchez, D. H. Powell, H. Dai and W. Tan, *J. Am. Chem. Soc.*, 2010, **132**, 17408.
92. F. Chen, Q. Qing, J. Xia, J. Li and N. Tao, *J. Am. Chem. Soc.*, 2009, **131**, 9908.
93. I. Willner and M. Zayats, *Angew. Chem. Int. Ed.*, 2007, **46**, 6408.
94. R. Stine, J. T. Robinson, P. E. Sheehan and C. R. Tamanaha, *Adv. Mater.*, 2010, **22**, 5297.
95. J. Wang, W. W. Zhao, X.-R. Li, J. J. Xu and H. Y. Chen, *Chem. Commun.*, 2012, **48**, 6429.
96. G. Yang, L. Li, R. K. Rana and J. J. Zhu, *Carbon*, 2013, 61, 357.
97. L. Zhao, S. Li, J. He, G. Tian, Q. Wei and H. Li, *Biosens. Bioelectron.*, 2013, **49**, 222.
98. R. Feng, Y. Zhang, H. Ma, D. Wu, H. Fan, H. Wang, H. Li, B. Du and Q. Wei, *Electrochim. Acta*, 2013, **97**, 105.

99. S. Deng, J. Lei, Y. Huang, Y. Cheng and H. Ju, *Anal. Chem.*, 2013, **85**, 5390.
100. Z. Qian, X. Shan, L. Chai, J. Ma, J. Chen and H. Feng, *ACS Appl. Mater. Inter.*, 2014, **6**, 6797.
101. W. Li, Z. Zhang, B. Kong, S. Feng, J. Wang, L. Wang, J. Yang, F. Zhang, P. Wu and D. Zhao, *Angew. Chem. Int. Ed.*, 2013, **52**, 8151.
102. Yao Zheng, Yan Jiao, Lu Hua Li, Tan Xing, Ying Chen, Mietek Jaroniec and S. Z. Qiao, *ACS Nano*, 2014, **8**, 5290.
103. Y. Ito, W. Cong, T. Fujita, Z. Tang, and M. Chen, *Angew. Chem. Int. Ed.*, 2015, **54**, 2131.
104. D. Jiang, X. Du, Q. Liu, N. Hao, J. Qian, L. Dai, H. Mao, and K. Wang, *Chem. Commun.*, 2015, **51**, 4451.
105. M. Rein, N. Richter, K. Parvez, X. Feng, H. Sachdev, M. Kläui and K. Müllen, *ACS Nano*, 2015, **9**, 1360.
106. S. Li, D. Wu, C. Cheng, J. Wang, F. Zhang, Y. Su, and X. Feng, *Angew. Chem. Int. Ed.*, 2013, **125**, 12327.
107. W. He, C. Jiang, J. Wang, L. Lu, *Angew. Chem. Int. Ed.*, 2014, **53**, 9503.
108. S. Li, D. Wu, H. Liang, J. Wang, X. Zhuang, Y. Mai, Y. Su, and X. Feng, *ChemSusChem*, 2014, **7**, 3002.
109. E. Haque, M. M. Islam, E. Pourazadi, M. Hassan, S. N. Faisal, A. K. Roy, K. Konstantinov, A. T. Harris, A. I. Minettc and V. G. Gomes, *RSC Adv.*, 2015, **5**, 30679.
110. Y. Tian, Y. Liu, J. Zhao and Y. Ding, *RSC Adv.*, 2015, **5**, 34070.

